# Morphology Development in Shear Flows of Straight and Folded Molten Fibers

**D. F. Zhang, D. A. Zumbrunnen, and Y. H. Liu**
Laboratory for Materials Processing and Industrial Mixing, Dept. of Mechanical Engineering, Clemson University, Clemson, SC 29634

*The morphological evolution of straight and folded molten fibers in shear flows was systematically investigated. Shear flows represent local flow conditions within actual batch mixers and extruders. Folded fibers were of interest, since folding may occur during melt processing and since folded fibers resemble portions of more complex extended structures arising in polymer blends. A general, three-dimensional numerical model of the time-dependent fluid flows within the molten-fiber phase and major-phase fluid was developed. Interactions between both fluids via fully dynamical, three-dimensional interfaces were considered. The relation of morphological changes in the fibers to the flow field for specified interfacial tensions and viscosity ratios are presented.*

## Introduction

New and existing thermoplastic resins offer an opportunity to produce a variety of polymer blends with attractive mechanical properties, especially if desirable microstructures can be obtained directly by melt processing. During the manufacture of polymer blends with extruders and mixers, molten minor-phase bodies within a major-phase melt can be transformed during mixing at low minor-phase concentrations into a wide variety of shapes such as sheets and fibers. These shapes are most often regarded as intermediate structures since they often become fragmented until a dynamically stable dispersion of droplets results. However, if the characteristic dimensions of sheets and fibers formed *in-situ* become sufficiently small during processing, it may be desirable to capture them by solidification in order to enhance the strength or toughness of plastics (Li et al., 1995; Liu and Zumbrunnen, 1997). A primary purpose of the present article is therefore to improve understanding of how molten fibers, once formed, evolve and interact with a major-phase flow field.

Examples of fibers and sheets formed by melt processing and separated from a polymeric matrix by dissolution are shown in Figure 1. Fibers protrude from the ends of sheets that themselves are twisted and folded. It is evident that many morphological changes in geometrically complex fluidic structures occur simultaneously during melt processing. Prior studies of morphological changes to interfaces have pertained to quiescent or extensional flows, and to simple shapes such as droplets or long, straight fibers. These idealized studies have proven quite useful in our understanding physical mechanisms and anticipating changes to portions of more complex bodies that may resemble simpler shapes.

Manufacturing methods for polymer blends have developed largely independently of detailed theoretical analyses. Experimental methods, trial-and-error, and models of simplified configurations and Newtonian behavior are still principal design tools. Studies of changes in the interfaces between fluids date to the pioneering work of Taylor (1934), who experimentally investigated the deformation of drops by a shear or an extensional flow in a surrounding fluid. When the viscous flow stress was greater than stresses associated with interfacial tension, drops elongated and sometimes broke. Results for these flows were later presented systematically by Bentley and Leal (1968) in terms of the phase viscosity ratio $C_\mu$, the capillary number, and the characteristics of the flow field. The breakup of liquid threads in a quiescent fluid has also been studied numerically by Stone and Leal (1989), who used a boundary-integral method. It was shown that internal flows developed, which resulted in the formation of bulbs at the thread ends. The bulbs enlarged until they became separated and formed droplets. The formation of droplets at the thread ends preceded breakup along the thread length by capillary instabilities.

Correspondence concerning this article should be addressed to D. A. Zumbrunnen.

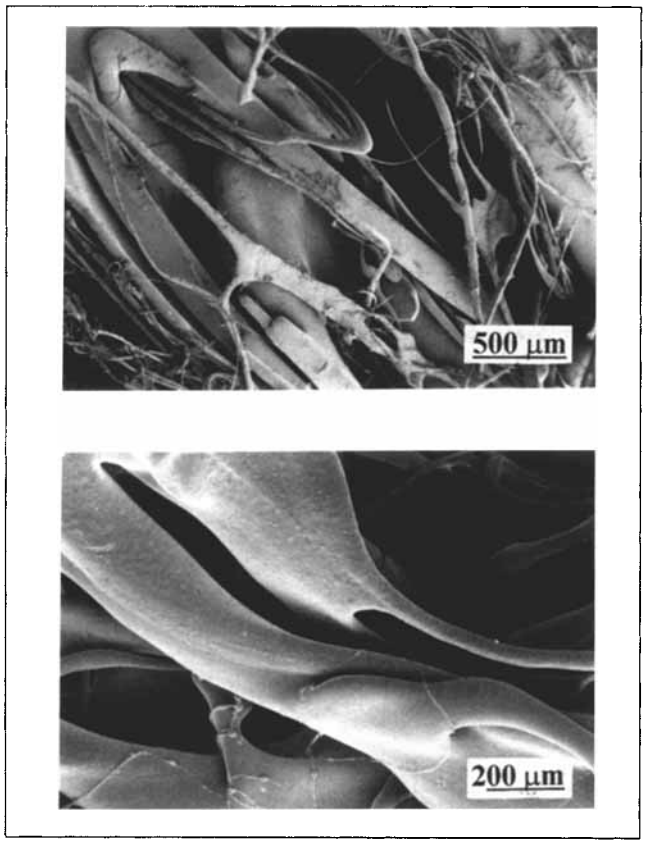


**Figure 1. Examples of low-density polyethylene structures formed by chaotic mixing at a concentration of 10% by volume with polystyrene with $C_\mu = 0.3$ and $\sigma = 0.005$ N/m (Liu and Zumbrunnen, 1996).**

Although Taylor's results and more recent related studies such as those briefly described earlier form the basis for much of our current understanding of the mechanisms leading to the formation of drops and fibers within polymer melts (Wu, 1987), investigations with non-Newtonian fluids have also been performed. Elmendorp (1986) used a hot-stage microscope and a video system to investigate changes to liquid polymer threads embedded in another molten polymer that was at rest. Breakup times for polymer melts were large compared to those for common liquids, due to high viscosities and low interfacial tensions. It was concluded that the effects of elasticity and shear thinning were negligible since deformation rates were very small. Breakup processes were essentially the same as for the Newtonian threads investigated by (Tomotika, 1935), and the results of studies with Newtonian fluids were deemed to be representative. However, while quiescent flow conditions may exist prior to the solidification of blends in molds, significant added complexities arise during extrusion and mixing where flows are subjected to external forcing. In these industrial processes, the phase viscosity ratio $C_\mu$, the capillary number, and time scales for deformation, breakup, and solidification have been proposed as pertinent parameters in order to anticipate at least qualitatively interfacial morphologies of polymer blends (Shi and Utracki, 1992). For example, fibrils that are formed at a high capillary number from droplets might be captured during a subsequent solidification process if the cooling time is shorter than the time scale for breakup. More recently, a new mathematical model of morphology development has been described where specific morphologies as blending proceeds are represented by a statistical measure (Wetzel and Tucker, 1997). In this model, an area tensor that is related directly to the local geometries of interfaces between fluids over a specified averaging volume is defined and calculated. Statistical techniques such as this one are in the early stages of development and may provide an efficient means to predict the future local blend morphology in response to complex flow fields.

Liquid-crystal polymer fibrils have been formed in a thermoplastic by blending in a single-screw extruder at low concentrations (Verhoogt et al., 1993, 1994). When captured by solidification, substantial increases in modulus of elasticity and tensile strength have been documented. The LCP fibrils subdivided into droplets if the fibrils remained in the molten state longer than the time needed for breakup. The resulting droplet morphologies were associated with poor mechanical properties. Fiberlike structures have been found to be the outcome of enlarging holes in sheets formed initially from resin pellets due to the strong shear environments characteristic of extruders. These fibers subsequently broke into droplets if blending was continued (Sundararaj et al., 1992; Scott and Macosko, 1995). In a study of blend morphology, the continuous transformation of large polystyrene bodies into thin elongated domains in low-density polyethylene has been observed in a convergent channel (David et al., 1993) where interfacial tension was lessened by the addition of a compatibilizer. The elongated domains were unstable and fragmented into droplets if not captured in time by solidification. Chaotic mixing has been used to create processing conditions conducive to progressive structure formation within immiscible thermoplastic melts (Zumbrunnen et al., 1996; Liu and Zumbrunnen, 1996). Under chaotic mixing conditions, individual fluid particles moved along unique paths so that minor-phase bodies were rapidly stretched and folded. A cylindrical, 1-cm-dia. minor-phase body was transformed initially to multitudinous and well-distributed lamellae. The lamellae subdivided into fibrils due to interfacial instabilities, and were subsequently captured by solidification. Low-density polyethylene at a concentration of only 9% by volume was recently combined with polystyrene by this method and toughness was enhanced by 69% (Liu and Zumbrunnen, 1997). This significant enhancement was attributed to a novel intertwined fibrous microstructure.

As suggested by these studies, finer fibrillar microstructures, greater microstructural uniformity, and improved processing equipment might be obtained for polymer blends, with greater understanding of the stability of evolving interfacial morphologies to imposed flow fields. In addition, morphological changes to filaments are also of general fundamental interest. A three-dimensional numerical model of the time-dependent flow fields within a minor phase and a major phase was therefore developed and implemented in this study to investigate morphological changes to straight and folded molten fibers formed during melt processing where the local flow field was given by a constant velocity gradient. The techniques that were used have been recently characterized as state of the art in a comprehensive review of the application

of Eulerian methods to moving interface problems (Shyy et al., 1996). Shear flows represent local conditions within extruders or mixers, and the folding of fibers is a common occurrence in blending. Results provide useful insights into how molten fibers, once formed *in situ*, response to local flow fields for specific phase properties. Morphological changes to fibers other than straight fibers are examined for closer relation to actual blending operations. Interactions between the minor and major phase fluids via fully dynamical, three-dimensional interfaces were considered. The model was validated by comparison to results of prior studies of droplet relaxation and fiber breakup in quiescent fluids.

## Governing Equations and Numerical Modeling

Numerical modeling was performed under conditions pertaining to the following assumptions: (1) unsteady, laminar flow; (2) constant properties; (3) immiscible fluids; (4) incompressible, Newtonian fluids; (5) no-slip conditions at fluid interfaces; (6) absence of gravitational or other external body forces. Neglecting shear-thinning and viscoelasticity effects was deemed appropriate given that results for Newtonian fluids were not available and since Newtonian models can provide pertinent information regarding morphology development, as was demonstrated in prior studies. The computational domain and applicable velocity boundary conditions are shown in Figure 2. A minor-phase fluid B fiber, with mass density $\rho_B$ and viscosity $\mu_B$, was initially suspended in the major-phase fluid $A$ of mass density $\rho_A$ and viscosity $\mu_A$. Both straight and folded fibers were considered. The initial shape of a typical folded fiber specified in the numerical model is shown in cross section in the plane $Z = W/2$. The folded fiber was composed of two long straight threads connected by a circular bend. The right portions of all fibers were contained within the computational domain, which had moving upper and lower surfaces and a corresponding steady shear flow at the left and right surfaces.

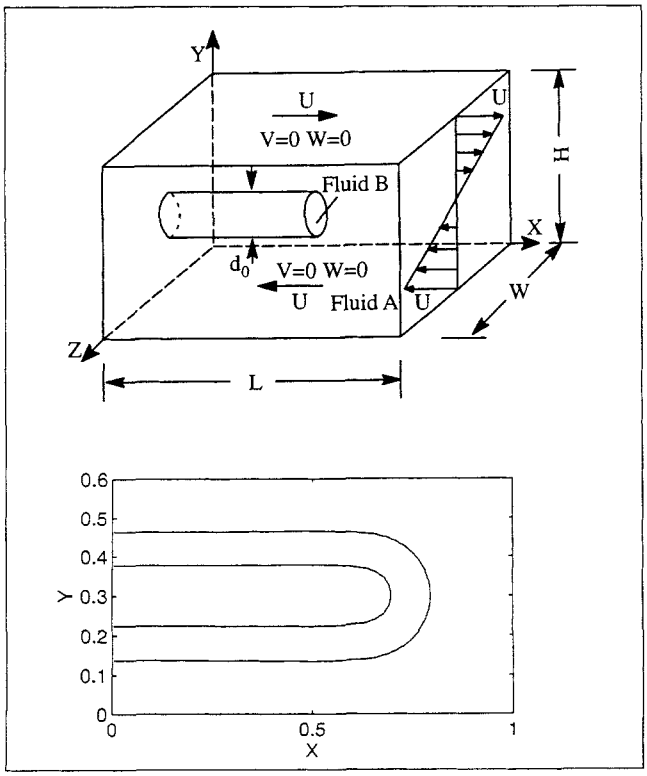


**Figure 2. Computational domain with applicable boundary conditions and cross-sectional view ($Z = W/2$) of the initial shape of the folded fiber.**

A primary task of this study was to construct a numerical model capable of predicting changes to three-dimensional fluid interfaces where viscous and interfacial forces are taken into account. A two-dimensional Eulerian model, which had been used recently in a fundamental study of fluid mixing (Zhang and Zumbrunnen, 1996), was modified for this purpose. Mathematical details for extending the model to three-dimensional interfaces have been presented by Zhang (1996). With regard to locating the interface, the volume-of-fluid (VOF) method (Hirt and Nichols, 1981) was selected since it overcomes ambiguities in interface locations and computational inefficiencies inherent in other methods by associating with the interface one-scalar function $f(X,Y,Z,t)$. The function $f$ was defined as the fractional volume of a computational cell occupied by the minor phase fluid $B$ of the fiber. Cells with $f$ values between zero and one then identified interface locations. Thus, the VOF method provided interface information with computational storage requirements consistent with other dependent variables.

Reconstruction of interfaces is often performed at each time step in order to determine and assign interfacial forces. Such reconstructions are computationally expensive. Recently, a two-dimensional continuum-surface-force (CSF) technique for modeling interfacial tension was introduced by Brackbill et al. (1992). The CSF technique is valid for moving interfaces between incompressible fluids where the interfacial tension coefficient is constant. In this method, interfacial tension is interpreted as a continuous, three-dimensional effect across an interface, rather than a boundary condition on the interface. Interfacial forces can thereby by replaced by an equivalent volumetric force $\boldsymbol{B}_{sv}(\boldsymbol{x})$. As a consequence, the CSF technique is ideally suited for Eulerian interfaces that are not in general aligned with the computational grid. The volumetric force $\boldsymbol{B}_{sv}(\boldsymbol{x})$ was related to the volume fraction $f$ according to

$$\boldsymbol{B}_{sv}(\boldsymbol{x}) = \sigma\kappa(\boldsymbol{x})\frac{\nabla f(\boldsymbol{x})}{[f]}. \tag{1}$$

In Eq. 1, $[f] = f_2 - f_1 = 1 - 0 = 1$, given the physical definition of $f$. The $x$, $y$, and $z$ components of $\boldsymbol{B}_{sv}(\boldsymbol{x})$ were then given by:

$$B_{svx}(\boldsymbol{x}) = \sigma\kappa(\boldsymbol{x})\frac{\partial f(\boldsymbol{x})}{\partial x}, \tag{2a}$$

$$B_{svy}(\boldsymbol{x}) = \sigma\kappa(\boldsymbol{x})\frac{\partial f(\boldsymbol{x})}{\partial y}, \tag{2b}$$

$$B_{svz}(\boldsymbol{x}) = \sigma\kappa(\boldsymbol{x})\frac{\partial f(\boldsymbol{x})}{\partial z}. \tag{2c}$$

The interface curvature $\kappa(x)$ in Eq. 2 can be expressed as the divergence of the unit-normal vector $\hat{n}(x)$ of the interface at $x$ (Kothe et al., 1991):

$$\kappa(x) = -[\nabla \cdot \hat{n}(x)] = \frac{1}{|n|}\left[\left(\frac{n}{|n|}\cdot\nabla\right)|n| - (\nabla \cdot n)\right]. \quad (3)$$

The normal vector $n(x)$ of the interface was obtained by the gradient of $f$,

$$n(x) = \nabla f = \left(\frac{\partial f}{\partial x}\right)\hat{i} + \left(\frac{\partial f}{\partial y}\right)\hat{j} + \left(\frac{\partial f}{\partial z}\right)\hat{k}. \quad (4)$$

More information about the CSF technique is available in recent papers (Kothe et al., 1991; Richards et al., 1993; Zhang and Zumbrunnen, 1996; Zhang, 1996).

With interfacial forces obtained from the VOF method and the CSF technique, the continuity and momentum equations in Cartesian coordinates were nondimensionalized in terms of suitable dimensionless parameters and variables (see the Notation section). Since investigations of capillary instabilities commonly pertain to low Reynolds numbers ($Re$), the scale factor $P_0$ for pressure pertained to viscous forces instead of inertial forces, for example. Additionally, the initial fiber diameter $d_0$ was used to nondimensionalize the interface curvature $\kappa$. The resulting dimensionless equations are given below.

$$\frac{\partial U}{\partial X} + \frac{1}{A_y}\frac{\partial V}{\partial Y} + \frac{1}{A_z}\frac{\partial W}{\partial Z} = 0 \quad (5)$$

$$Re\left(\frac{\partial (MU)}{\partial \tau} + U\frac{\partial (MU)}{\partial X} + \frac{1}{A_y}V\frac{\partial (MU)}{\partial Y} + \frac{1}{A_z}W\frac{\partial (MU)}{\partial Z}\right)$$
$$= -\frac{\partial P}{\partial X} + A_R\sigma^* K\frac{\partial f}{\partial X} + \frac{\partial}{\partial X}\left(\Gamma\frac{\partial U}{\partial X}\right) + \frac{1}{A_y^2}\frac{\partial}{\partial Y}\left(\Gamma\frac{\partial U}{\partial Y}\right)$$
$$+ \frac{1}{A_z^2}\frac{\partial}{\partial Z}\left(\Gamma\frac{\partial U}{\partial Z}\right) \quad (6)$$

$$Re\left(\frac{\partial (MV)}{\partial \tau} + U\frac{\partial (MV)}{\partial X} + \frac{1}{A_y}V\frac{\partial (MV)}{\partial Y} + \frac{1}{A_z}W\frac{\partial (MV)}{\partial Z}\right)$$
$$= -\frac{1}{A_y}\frac{\partial P}{\partial Y} + \frac{A_R}{A_y}\sigma^* K\frac{\partial f}{\partial Y} + \frac{\partial}{\partial X}\left(\Gamma\frac{\partial V}{\partial X}\right)$$
$$+ \frac{1}{A_y^2}\frac{\partial}{\partial Y}\left(\Gamma\frac{\partial V}{\partial Y}\right) + \frac{1}{A_z^2}\frac{\partial}{\partial Z}\left(\Gamma\frac{\partial V}{\partial Z}\right) \quad (7)$$

$$Re\left(\frac{\partial (MW)}{\partial \tau} + U\frac{\partial (MW)}{\partial X} + \frac{1}{A_y}V\frac{\partial (MW)}{\partial Y} + \frac{1}{A_z}W\frac{\partial (MW)}{\partial Z}\right)$$
$$= -\frac{1}{A_z}\frac{\partial P}{\partial Z} + \frac{A_R}{A_z}\sigma^* K\frac{\partial f}{\partial Z} + \frac{\partial}{\partial X}\left(\Gamma\frac{\partial W}{\partial X}\right) + \frac{1}{A_y^2}\frac{\partial}{\partial Y}\left(\Gamma\frac{\partial W}{\partial Y}\right)$$
$$+ \frac{1}{A_z^2}\frac{\partial}{\partial Z}\left(\Gamma\frac{\partial W}{\partial Z}\right). \quad (8)$$

The dimensionless mass density $M$ and viscosity $\Gamma$ in Eqs. 6, 7, and 8 are properties of computational cells in which both fluid $A$ and fluid $B$ may be obtained. Given the fact that the sharp fluid $A/B$ interface is replaced with the CSF technique by a transition region, these two properties were obtained by linearly combining the properties of the two different fluids according to the volume fraction $f$:

$$M = 1 + f(C_\rho - 1) \quad (9)$$

$$\Gamma = 1 + f(C_\mu - 1). \quad (10)$$

Inertial-force terms were included in the governing equations in order to obtain a general model that can be used to investigate inertial effects. In melt processing to form structures *in-situ* (Liu and Zumbrunnen, 1996, 1997) and studies of extended drops (Stone and Leal, 1989; Stone, 1994), results pertained to Reynolds numbers on the order of unity. For consistency with these prior studies, the present calculations were performed with $Re = 1$ and $C_\rho = 1$.

Physically appropriate boundary conditions were specified as shown in Figure 2. Considering that a steady shear flow was imposed in the exterior major phase (fluid $A$) by the motion of the upper and lower surfaces, the nondimensional boundary conditions were prescribed by Eqs. 11a–11f.

$$X = 0, \quad U = 2(Y - 0.5), \quad V = W = 0 \quad (11a)$$
$$X = 1, \quad U = 2(Y - 0.5), \quad V = W = 0 \quad (11b)$$
$$Y = 0, \quad U = -1, \quad V = W = 0 \quad (11c)$$
$$Y = 1, \quad U = 1, \quad V = W = 0 \quad (11d)$$
$$Z = 0, \quad U = 2(Y - 0.5), \quad V = W = 0 \quad (11e)$$
$$Z = 1, \quad U = 2(Y - 0.5), \quad V = W = 0. \quad (11f)$$

Equations 6–8 were discretized using the finite-volume approach and were solved according to the SIMPLE method (Patankar, 1980) where the hybrid scheme (Spalding, 1972) was used to discretize advective and diffusive terms. A uniform mesh was used in the $X$, $Y$, and $Z$ directions in order to accurately discern morphology changes. A fully implicit formulation, using first-order backward differencing for temporal terms, was used to avoid instability problems. The volumetric forces were calculated using Eqs. 2a–2c and the mass density M and viscosity $\Gamma$ of computational cells were obtained from Eqs. 9 and 10, all of which were based on $f$ evaluated with the donor-acceptor algorithm at the previous time level.

The mesh was successively refined to ensure grid independence in the calculated instantaneous velocity fields and an acceptably small numerical uncertainty in the calculated positions of interfaces. The mesh was refined so that the calculated velocity components for a certain time at six unique reference points differed by less than 0.1%. The six reference points were located in the vicinity of the interfaces where three-dimensional variations in the velocity fields were greatest. To satisfy the second criterion, the mesh was refined until respective locations of a straight fiber with $\sigma^* = 5.0$, $C_\mu = 0.1$, and $d_0/L = 0.08$ differed by less than 1% after the maximum elapsed time. Meshes that satisfied both criteria were $100 \times 60 \times 30$ for $A_y = 0.6$ and $A_z = 0.3$. Time-step independence for both velocity and interface locations were assessed

by successively refining the time step $\Delta\tau$ until calculated values at each time step for the selected mesh size had relative differences of less than $10^{-5}$. For most cases, $\Delta\tau = 10^{-3}$ was selected. Iterations in the line-by-line, tridiagonal matrix algorithm within each time step were continued until two convergence criteria were satisfied. For the first convergence criterion, the maximum relative differences in velocity components in the entire computational domain were required to be less than $10^{-5}$. Second, the maximum mass-balance error of each computational cell was required to be less than $5 \times 10^{-5}$. The amount of CPU time on a Silicon Graphics, Inc. (Mountain View, CA) Onyx supercomputer (75 MFLOP) for the selected mesh size, time step, and convergence criteria ranged from 36 h to 72 h.

Several available experimental and numerical solutions were used to test the numerical accuracy and further validate the computational model. The stationary shape of a three-dimensional minor-phase body in a steady shear flow field was numerically simulated. The results with the VOF method in conjunction with the CSF technique were compared and found to be in good agreement with the experimental results of Bentley and Leal (1986) for stable, deformed droplets in two-dimensional shear flows. The relaxation and breakup of an initially extended drop in a quiescent surrounding fluid was also calculated and compared with the numerical results of Stone and Leal (1989). Calculated velocities both inside and outside the extended drop and the shapes of the interfaces were in excellent agreement.

## Results and Discussion

Prior to considering the evolution of fibers in steady shear flows, it is informative to first consider an example of the evolution of a straight fiber in an initially motionless immiscible fluid. This situation can be regarded as a special case of zero shear, such as may occur prior to solidifying molten fibers after melt processing has stopped. Changes to the fiber shape are shown in Figure 3 within the plane $Z = 0.5$ (Figure 2), and the velocity vectors in the different phases are overlaid. Fluid velocities remained small outside of the fiber so that velocity vectors appear as very short arrows. The two-phase flow near the fiber surface was interfacially driven so that larger velocities arose within the fiber shaft. The magnitude of the interfacial tension played no qualitative role in the interfacial evolution, but only determined the dimensional time scale (Stone and Leal, 1989). It is clear that a flow was induced early in the transient near the fiber end by interfacial tension as the fiber attempted to relax to an equilibrium form. Morphological changes to the fiber can be explained for the quiescent flow in terms of the equilibrium pressure $P_s$ (Brackbill, et al., 1992; Carey, 1992) required to balance interfacial forces. In a two-dimensional cylindrical thread such as the central part of the fiber, $P_s = \sigma/R$. In a three-dimensional case, $P_s = 2\sigma/R$. Consequently, the equilibrium pressure for a specific radius is larger for a three-dimensional bulb than for a two-dimensional fiber. Pertaining to the interface shapes in Figure 3, the interface near the end of the fiber where the shape is three-dimensional moved inward since the internal pressure was below $P_S$. The inward flow led to an accumulation of fluid and the formation of a bulb. Due to the uniformity of the adjacent fiber shape, there was no

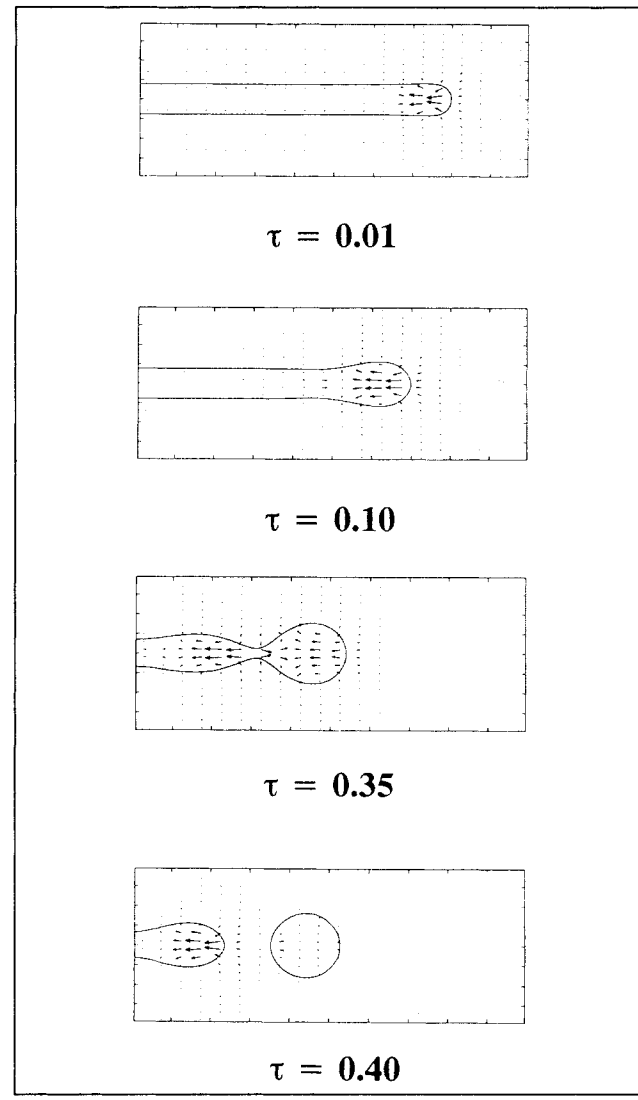


**Figure 3. Cross-sectional views ($Z = W/2$) of end-pinching of a straight fiber in an initially motionless fluid with $d_0/L = 0.08$, $\sigma^* = 5.0$, and $C_\mu = 0.10$.**

detectable flow in the central region for $\tau < 0.10$. The region connecting the bulb and the central part will subsequently be referred to as the *adjoining region*. In the adjoining region, the interface showed strong two-dimensionality and had a larger radius than the main fiber body due to the proximity of the bulb. A weak flow resulted from the central portion toward the fiber end into the bulb, which eventually collided with the inward flow associated with the bulb formation. The onset of this flow pattern in quiescent fluids ($\tau = 0.10$) has been regarded as the beginning of end-pinching and led to the formation of the thin neck at $\tau = 0.35$. Thin necks such as this one are known as a *pinch* (Stone and Leal, 1989). The equilibrium pressure within the neck became high as the neck radius decreased. Flows were consequently induced away from the neck until the fiber end pinched off and a droplet was formed. At larger dimensionless times, new adjoining regions arose and the process repeated along the remaining fiber shaft.

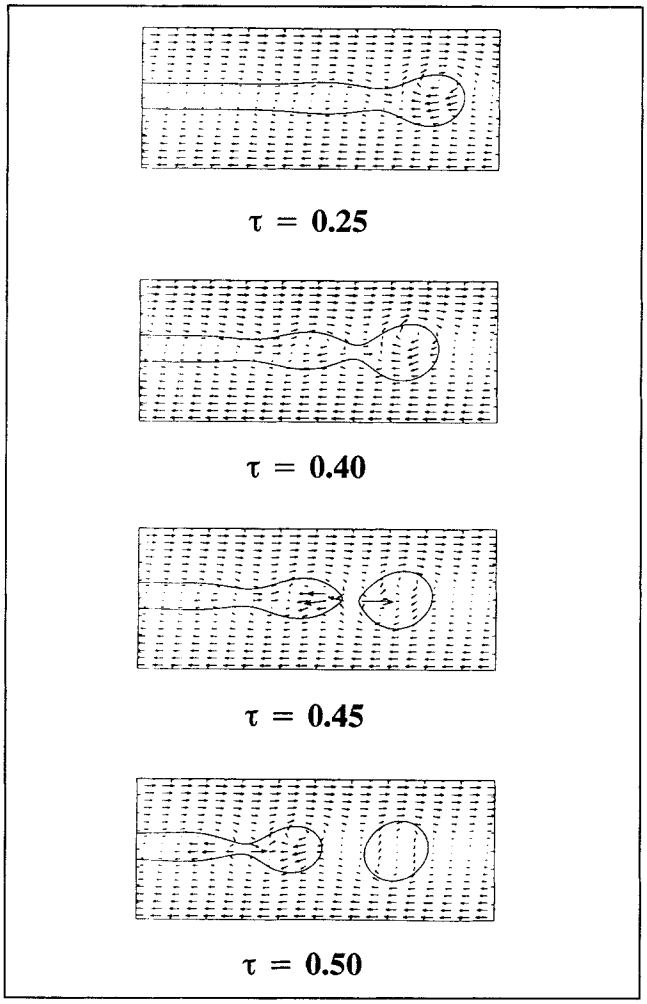


**Figure 4. Cross-sectional views ($Z/=W/2$) of morphological changes to a straight fiber in a steady shear flow with $d_0/L=0.08$, $\sigma^*=5.0$, and $C_\mu=0.10$.**

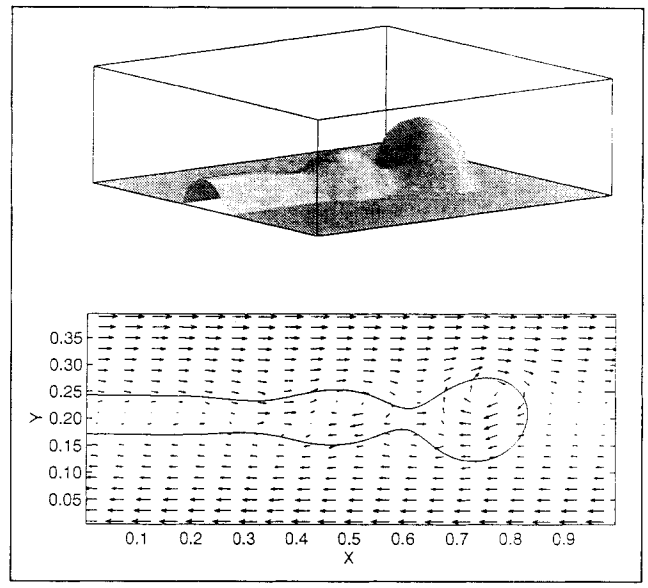


**Figure 5. Three-dimensional view of a straight fiber and the corresponding velocity fields at $Z=W/2$ for $\tau=0.40$, $d_0/L=0.08$, $\sigma^*=5.0$, and $C_\mu=0.10$.**

The preceding discussion of end-pinching pertained to a quiescent fluid. During melt processing, however, microstructures are formed as a result of interactions between active interfaces and imposed flow fields. The evolution of a straight fiber in a steady shear flow is therefore shown in Figure 4. The two-phase flow in the vicinity of the fiber was no longer interfacially driven alone. Instead, it was also the result of shear stresses and an external pressure field. With $\sigma^*=5.0$, interfacial tension forces remained dominant, however. The imposed shear flow acted to deform the fiber while interfacial tension tended to resist deformations. Interfacial tension also attempted to breakup the fiber end through end-pinching owing to the nonequilibrium shape of the fiber end as discussed earlier. Comparing Figure 4 with the quiescent fluid case (Figure 3), it is clear that the shear stress arising from the imposed shear flow induced changes to the fiber shape. Symmetry about the fiber axis was lost as a result of the shear flow. In order to provide an overall picture of the fiber surface, three-dimensional and expanded cross-sectional views for Figure 4 at $\tau=0.40$ are shown in Figure 5. The shear velocity field (Figure 2) adjacent to the fiber was significantly altered due to interfacial interactions. The more complex fiber shape allowed less organized internal flows and internal pressure variations. As a consequence, end-pinching was slowed and the fiber was more readily preserved due to the shear flow. Stationary and rotating elliptic droplets were finally formed as shown in Figure 4 at $\tau=0.50$. The formation of stable elliptic droplets in steady shear flows has been observed both experimentally and numerically by other researchers (Bentley and Leal, 1986).

Figure 6 demonstrates the evolution of a straight fiber with a smaller interfacial tension ($\sigma^*=2.0$). Due to the smaller interfacial tension, the influence of shear stress relative to interfacial tension was greater than for cases shown in Fig-4 and 5. End-pinching did not occur and instead a stationary shape was evolved at the fiber end. It is interesting to note that the flow fields in the two phases near the fiber were still altered by interfacial interactions and a strong circulation can be clearly observed within the fiber end. An overall force balance and a stationary interface was reached at $\tau=0.75$ between interfacial tension forces and flow shear stresses at both the exterior and internal fiber surfaces. At a lower interfacial tension ($\sigma^*=0.5$), the shear stress became the predominant factor and the fiber was continuously stretched without breakup (Zhang, 1996). These results demonstrate that additives, such as compatibilizers in polymeric systems that reduce interfacial tension, can be effective in promoting the formation of higher aspect-ratio fibers during melt processing. Solidification times can also be longer for melts with lower interfacial tensions, since end-pinching proceeds more slowly as explained in conjunction with Figure 3.

The foregoing discussion pertained to straight portions of fibers. Such straight fibers can in general become folded or connected to other shapes during melt processing. The evolution of a folded fiber is given in Figure 7 for a quiescent fluid with conditions otherwise identical to those of Figure 3. It is clear that the two-phase flows around the folded fiber were

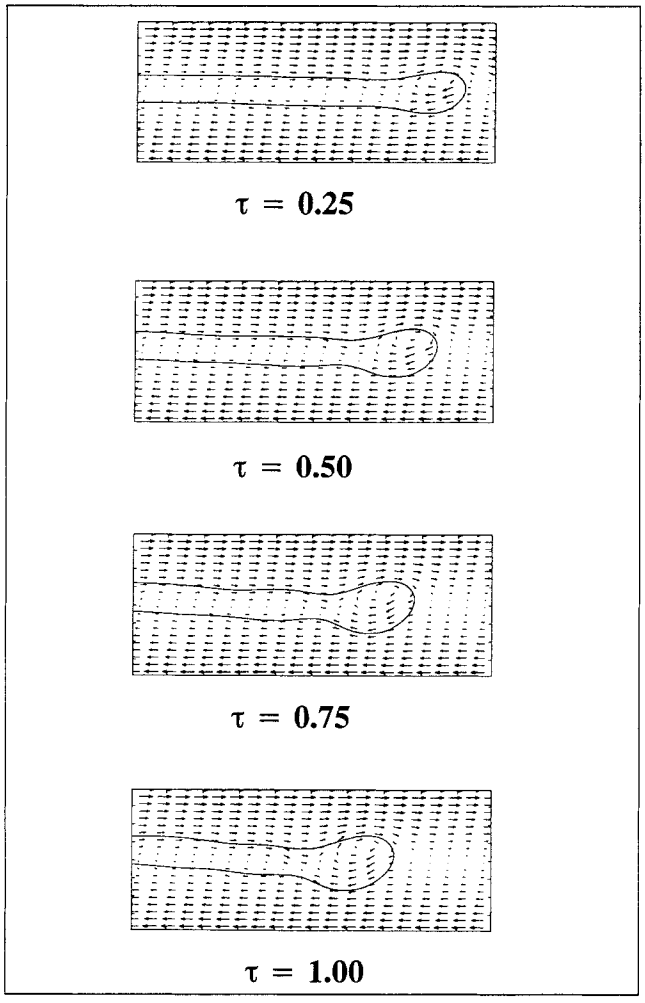


**Figure 6. Cross-sectional views ($Z = W/2$) of morphological changes to a straight fiber in a steady shear flow with $d_0/L = 0.08$, $\sigma^* = 2.0$, and $C_\mu = 0.10$.**

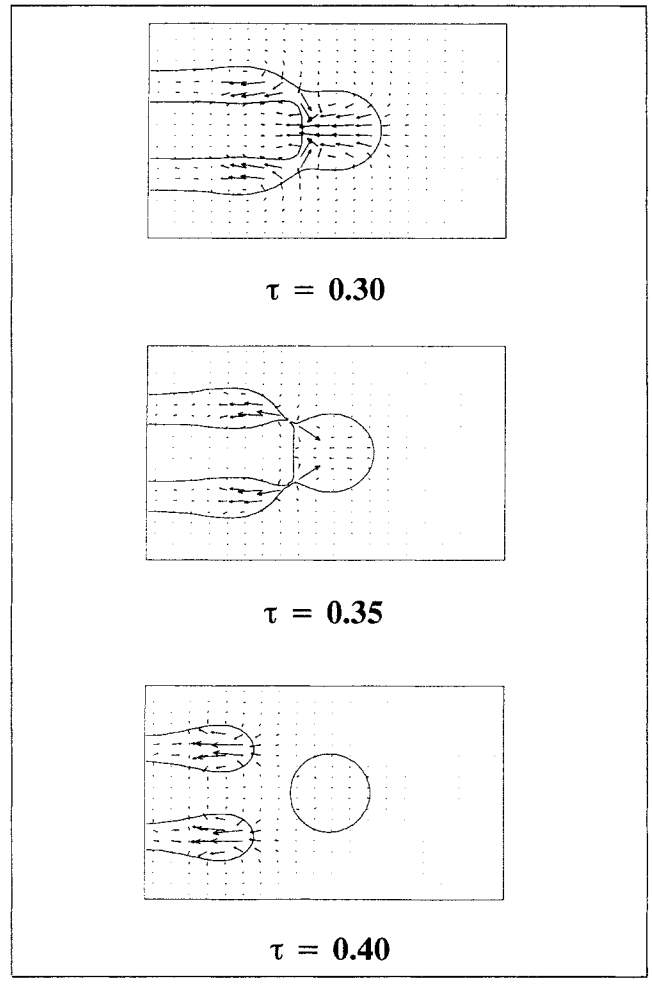


**Figure 7. Cross-sectional views ($Z = W/2$) of end-pinching in a folded fiber in a quiescent fluid with $d_0/L = 0.08$, $\sigma^* = 5.0$, and $C_\mu = 0.10$.**

interfacially driven as in the end-pinching process for straight fibers. Since the folded portion was not an equilibrium form, the fluid in the fold was driven by interfacial tension so that a net motion occurred toward the unfolded parts. The fluid located in the inner portion of the fold was propelled faster by the interface due to larger curvatures where a higher value of equilibrium pressure $P_s$ would be required to maintain the interface shape. Fluid motion also occurred in the adjoining regions. As a result of these motions, two necks were formed very soon at $\tau = 0.30$. It was shown previously that the formation of necks portends end-pinching in a quiescent fluid. As the necks became better defined, end-pinching was accelerated. Breakup was evident at $\tau = 0.35$.

Comparing the end-pinching process associated with the folded fiber in Figure 7 with that occurring for a long straight fiber in Figure 3, it is interesting to observe that end-pinching occurred more rapidly in the folded end. This result is consistent with the experimental results obtained by Tjahjadi and Ottino (1991) in a study of stretched and folded droplets in a chaotic mixing environment. After breakup, the folded portion was transformed into a spherical droplet at $\tau = 0.40$. The size of the droplet relative to the fiber diameter depended principally on the outer diameter of the fold since the droplet was derived from the fold itself. A larger fold corresponded to a larger droplet. Compared with the droplet separated from the straight fiber in Figure 3, the droplet associated with the fold was larger. After separating from the folded portion, end-pinching also occurred in the two resulting straight fibers in the manner described earlier for straight single fibers. Evidence of this end-pinching can be seen in Figure 7 at $\tau = 0.40$. These results demonstrate that observed differences in droplet sizes within polymer blends where a fibrillar structure is promoted arise in part due to the presence of folds in extended fibers.

The evolution of a typical folded fiber in a steady shear flow is shown in Figure 8 for conditions otherwise identical to those of Figure 7. End-pinching still occurred but in a manner differing from the one for a quiescent surrounding fluid. Due to the effect of the imposed shear flow, the interfacial morphological evolution was not symmetrical. Breakup first occurred in the lower folded portion of the fiber where the imposed shear flow acted in tandem with interfacially driven flows. The pressure distribution associated with the interfa-

cial forces at the folded end led to fluid motion toward the straight part of the folded fiber. At the same time, an outward fluid motion toward the end arose in the adjoining region as in the case for the quiescent fluid. As a result, two necks were formed. In response to the imposed shear flow, the sizes of the two necks differed. This difference was most apparent at $\tau = 0.25$ in Figure 8.

The effect of interfacial tension on the evolution of a folded fiber in steady shear flows is demonstrated in Figure 9 for $\tau = 0.75$. Unlike the case for the single straight fiber with $\sigma^* = 2.0$ in Figure 6, end-pinching still occurred in the lower fiber after breakup of the fold. However, unlike in Figure 8, the fold breakup was not accompanied by the formation of a separate droplet. In addition, stable fiber shapes were not formed, since the shear flow field was significantly altered between the straight portions of the folded fiber. The velocity field in this region resulted from the flow fields within the fiber and the interfacial motion. An equilibrium force balance could not arise as occurred in Figure 6, where the shear flow field acted on a single fiber. For $\sigma^* = 0.50$, the influence of the interfacial tension was small and changes in the

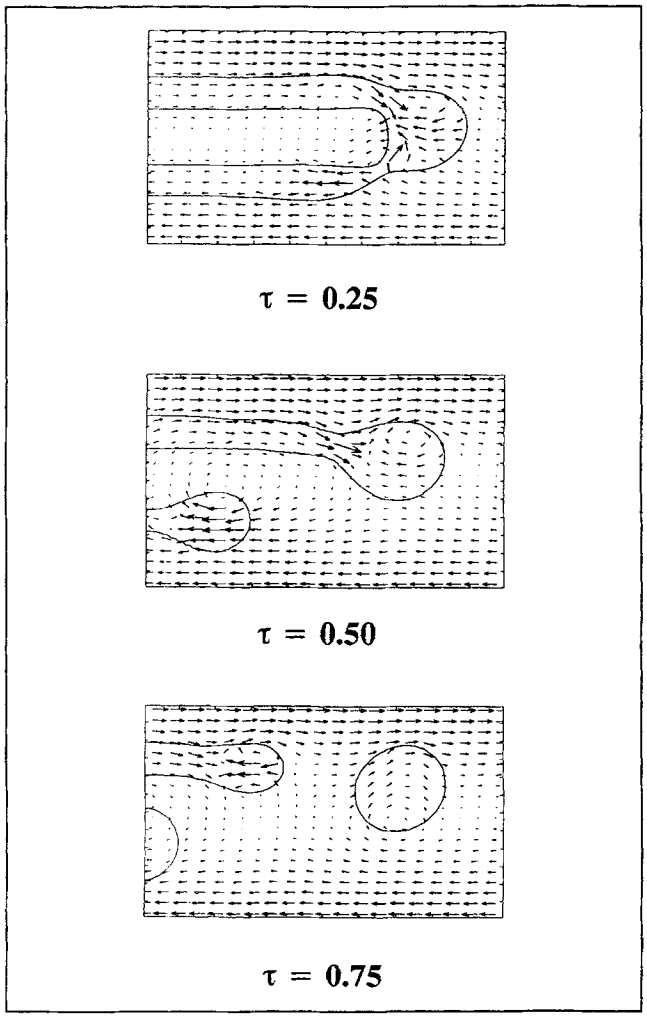


**Figure 8. Cross-sectional views ($Z = W/2$) of morphological changes to a folded fiber in a steady shear flow with $d_0/L = 0.08$, $\sigma^* = 5.0$, and $C_\mu = 0.10$.**

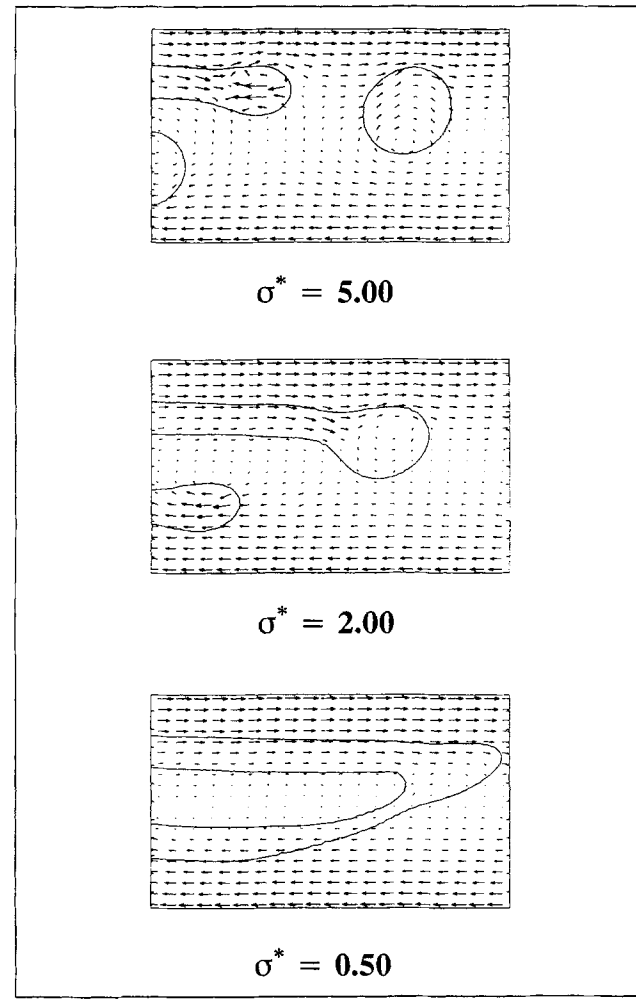


**Figure 9. Effect of interfacial tension on morphological changes to a folded fiber in a steady shear flow with $\tau = 0.75$, $d_0/L = 0.08$, and $C_\mu = 0.10$.**

fiber shape were primarily dependent on the external flow field. Further computations up to $\tau = 1.00$ showed that the folded fiber continued to deform due to the shear flow without breakup even though the fold diameter decreased continuously. These results demonstrate that straight and folded molten fibers can be effectively stretched in shear flows that arise during melt processing without breakup if interfacial tension is low. Folding also makes unlikely the formation of equilibrium structures even in steady shear flows.

The effect of the phase-viscosity ratio $C_\mu$ on the evolution of a folded fiber is shown in Figure 10 for $\sigma^* = 2.0$. A smaller phase-viscosity ratio generally promoted end-pinching near the folded end. This result has also been shown to be valid for straight fluid filaments in a quiescent fluid (Stone and Leal, 1989). For a very small phase-viscosity ratio ($C_\mu = 0.01$), the folded end and the subsequently separated straight fibers were entirely broken up. For $C_\mu = 0.1$, induced shear stresses were comparable to interfacial tension. The folded end was broken but the two separated straight fibers resisted end-pinching so that two stable bulbous ends were formed. For $C_\mu = 1.00$, shear stresses became very strong compared to interfacial tension. Breakup near the folded end occurred

eventually for $\tau \approx 1.0$ as the lower portion of the fiber was stretched. For $C_\mu = 5.0$, shear stresses were predominant and the folded fiber deformed continuously without breakup for the maximum dimensionless time of the computations ($\tau = 1.0$). The formation of long, continuous fibers by melt processing with phases where high interfacial tension exists can thereby be most effectively accomplished at higher viscosity ratios. It is interesting to note that similar fiber structures can be obtained by independently controlling either interfacial tension or phase viscosity ratio, as a comparison of Figures 9 and 10 indicates. Since the viscosities of thermoplastic polymers depend strongly on temperature, phase viscosity ratios that promote the continued refinement of extended fibers as in Figure 10 might be obtained by carefully selecting the processing temperature even when interfacial tension cannot be effectively reduced by the addition of compatibilizers to the melt.

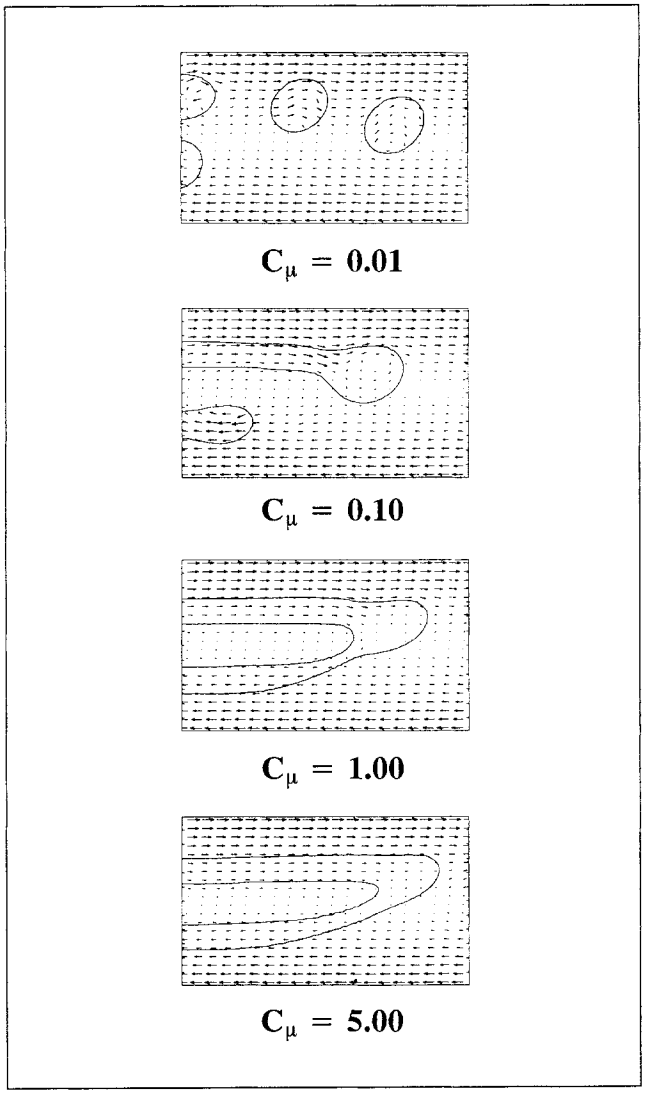


**Figure 10. Effect of phase viscosity ratio on morphological changes to a folded fiber in a steady shear flow with $\tau = 0.75$, $d_0/L = 0.08$, and $\sigma^* = 2.0$.**

## Conclusions

After validation by comparison with results of prior experiments, a computationally efficient, three-dimensional numerical model was used to determine changes to interfacial morphologies of extended straight and folded fibers due to an imposed external shear flow in a surrounding fluid. This situation represented local conditions during melt processing where it is often desirable to evolve fibers in a minor-phase melt to achieve strength or toughness enhancement in solidified parts. Folded fibers subjected to steady shear flows were stretched and breakup occurred preferentially within the fold by end-pinching. Comparing the end-pinching process associated with a folded fiber with that occurring for a long straight fiber, end-pinching was promoted by the folded end and occurred first on the side of the fold where the shear aided the formation of a neck. End-pinching in both straight and folded fibers was delayed by the imposed shear flow since internal flows were less organized within the more complex fiber shapes that arose. As a consequence, fibers were more readily preserved when acted on by shear flows. Morphological changes depended strongly on phase-viscosity ratio and interfacial tension. Straight and folded fibers were readily lengthened by external shear forces without breakup when interfacial tension was very small or when the phase-viscosity ratio was sufficiently large to attenuate instabilities. However, at high interfacial tensions, flows in the vicinity of folded fibers became interfacially driven until bulbous ends in folds were formed that, subsequently separated from the fiber to yield two shorter fibers. These shorter fibers subdivided by end-pinching to form elliptic droplets in the shear flow. Larger droplets were also produced by the breakup of folds with sizes proportional to the outer diameter of a fold. The formation of both small and large drops by the breakup of folded fibers provides one explanation for droplet-size variability in solidified melts. Unlike for straight fibers, stable shapes could not be formed in folded fibers, since the flow field was significantly altered in the region between the shafts of the folded fiber. Thus, fiber folding tends to hasten subsequent morphological changes.

## Acknowledgments

Support for this work was provided by the National Science Foundation under Grant CMS-9253640 in conjunction with a Presidential Faculty Fellow Award to one of the authors (D. A. Z.), and is gratefully acknowledged.

## Notation

$A_R$ = ratio of initial fiber diameter to computational domain length = $d_0/L$
$A_y$ = aspect ratio of the computational domain = $H/L$
$A_z$ = aspect ratio of the computational domain = $W/L$
$C_\rho$ = ratio of density of minor phase $B$ to the density of the major phase $A = \rho_B/\rho_A$
$H$ = height of computational domain
$L$ = length of computational domain
$P$ = dimensionless pressure = $p/P_0$
$p$ = pressure (N/m$^2$)
$t$ = time (s)
$T_0$ = scale factor for time = $L/u_0$
$u$ = velocity component in $x$-direction (m/s)
$u_0$ = scale factor for velocity = $\nu/L$ (m/s) for quiescent flow or velocity of moving wall for shear flow (Figure 2)
$U$ = dimensionless velocity component in $x$-direction = $u/u_0$

$v$ = velocity component in $y$-direction (m/s)
$V$ = dimensionless velocity component in $y$-direction = $v/u_0$
$w$ = velocity component in $z$-direction (m/s)
$W$ = dimensionless velocity component in $z$-direction = $w/u_0$
$W$ = width of computational domain
$x$ = horizontal coordinate (m)
$X$ = dimensionless horizontal coordinate = $x/L$
$y$ = vertical coordinate (m)
$Y$ = dimensionless vertical coordinate = $y/H$
$z$ = crosswise coordinate (m)
$Z$ = dimensionless crosswise coordinate = $z/W$
$\tau$ = dimensionless time = $t/T_0$
$\nu$ = kinematic viscosity of major phase fluid $A$ ($m^2/s$)
$\sigma$ = interfacial tension (N/m)
$\sigma^*$ = dimensionless interfacial tension = $\sigma/\mu_A u_0$
K = dimensionless curvature of interface = $\kappa d_0$

## Literature Cited


Bentley, B. J., and L. G. Leal, "An Experimental Investigation of Drop Deformation and Breakup in Steady Two-Dimensional Linear Flows," *J. Fluid Mech.*, **167**, 241 (1986).

Brackbill, J. U., D. B. Kothe, and C. Zemach, "A Continuum Method for Modeling Surface Tension," *J. Comput. Phys.*, **100**, 335 (1992).

Carey, V. P., *Liquid-Vapor Phase Change Phenomena*, Hemisphere, Washington, DC, p. 86 (1992).

David, B., M. Kozlowski, and Z. Tadmor, "The Effect of Mixing History on the Morphology of Immiscible Polymer Blends," *Polym. Eng. Sci.*, **33**, 227 (1993).

Elmendorp, J. J., "A Study of Polymer Blending Microrheology," *Polym. Eng. Sci.*, **26**, 418 (1986).

Hirt, C. W., and B. D. Nichols, "Volume of Fluid (VOF) Method for the Dynamics of Free Boundaries," *J. Comput. Phys.*, **39**, 201 (1981).

Kothe, D. B., R. C. Mjolsness, and M. D. Torrey, "RIPPLE: A Computer Program for Incompressible Flows with Free Surfaces," Los Alamos National Laboratory Rep. LA-12007-MS, Los Alamos, NM (1991).

Li, G., J. Yin, B. Li, G. Zhuang, Y. Yang, and L. Nicolais, "In Situ Composite: Phenolphthalein Polyethersulfone-Thermotropic Liquid Crystalline Polymer Blends," *Poly. Eng. Sci.*, **35**, 656 (1995).

Liu, Y. H., and D. A. Zumbrunnen, "Emergence of Fibrillar Composites due to Chaotic Mixing of Molten Polymers," *Poly. Compos.*, **17**, 187 (1996).

Liu, Y. H., and D. A. Zumbrunnen, "Toughness Enhancement in Polymer Blends Due to the In-Situ Formation of Fine-Scale Extended Structures at Low Minor Phase Concentrations," *Proc. Int. Mechanical Engineering Congress and Exposition*, MD-80, 301, ASME, New York (1997).

Patankar, S. V., *Numerical Heat Transfer and Fluid Flow*, Hemisphere, New York (1980).

Richards, J. R., A. N. Beris, and A. M. Lenhoff, "Steady Laminar Flow of Liquid-Liquid Jets at High Reynolds Numbers," *Phys. Fluids*, **A5**, 1703 (1993).

Scott, C. E., and C. W. Macosko, "Morphology Development during the Initial Stages of Polymer-Polymer Blending," *Polymer*, **36**, 461 (1995).

Shi, Z. H., and A. Utracki, "Development of Polymer Blend Morphology during Compounding in a Twin-Screw Extruder: Part II: Theoretical Derivations," *Polym. Eng. Sci.*, **32**, 1834 (1992).

Shyy, W., H. S. Udaykumar, M. M. Rao, and R. W. Smith, *Computational Fluid Dynamics with Moving Boundaries*, Taylor & Francis, Washington, DC (1996).

Spalding, D. B., "A Novel Finite Difference Formulation for Differential Expressions Involving Both First and Second Derivatives," *Int. J. Numer. Methods Eng.*, **551** (1972).

Stone, H. A., and L. G. Leal, "Relaxation and Breakup of an Initially Extended Drop in an Otherwise Quiescent Fluid," *J. Fluid Mech.*, **198**, 399 (1989).

Stone, H. A., "Dynamics of Drop Deformation and Breakup in Viscous Fluids," *Ann. Rev. Fluid Mech.*, **26**, 65 (1994).

Sundararaj, U., and C. W. Macosko, "Drop Breakup and Coalescence in Polymer Blends: The Effects of Concentration and Compatibilization," *Macromolecules*, **28**, 2647 (1995).

Taylor, G. I., "The Formation of Emulsions in Definable Fields of Flow," *Proc. Roy. Soc. London*, **A146**, 501 (1934).

Tjahjadi, M., and J. M. Ottino, "Stretching and Breakup of Droplets in Chaotic Flows," *J. Fluid Mech.*, **232**, 191 (1991).

Tomotika, S., "On the Stability of a Cylindrical Thread of a Viscous Liquid Surrounded by Another Viscous Fluid," *Proc. Roy. Soc. London*, **A150**, 322 (1935).

Verhoogt, H., H. C. Langelaan, J. Van Dam, and A. Posthuma De Boer, "Blends of a Thermotropic Liquid Crystalline Polymer and a Thermoplastic Elastomer: I. Mechanical Properties and Morphology," *Poly. Eng. Sci.*, **33**, 754 (1993).

Verhoogt, H., C. R. J. Willems, J. Van Dam, and A. Posthuma De Boer, "Blends of a Thermotropic Liquid Crystalline Polymer and a Thermoplastic Elastomer: II. Formation and Stability of LCP Fibers," *Polym. Eng. Sci.*, **34**, 453 (1994).

Wetzel, E. D., and C. L. Tucker, III, "Area Tensors for Modeling Laminar Liquid-Liquid Mixing," *Tech. Rep. UILU-ENG 97-4014*, Univ. of Illinois, Urbana-Champaign (1997).

Wu, S. H., "Formation of Dispersed Phase in Incompatible Polymer Blends: Interfacial and Rheological Effects," *Poly. Eng. Sci.*, **27**, 335 (1987).

Zhang, D. F., "Development of Interfacial Morphologies during the Chaotic Mixing of Fluids," PhD Thesis, Clemson Univ., Clemson, SC (1996).

Zhang, D. F., and D. A. Zumbrunnen, "Chaotic Mixing of Two Similar Fluids in the Presence of a Third Dissimilar Fluid," *AIChE J.*, **42**, 3301 (1996).

Zumbrunnen, D. A., K. C. Miles, and Y. H. Liu, "Auto-Processing of Very Fine-Scale Composite Materials by Chaotic Mixing of Melts," *Composites Part A*, **27A**, 37 (1996).



*Manuscript received June 13, 1997, and revision received Sept. 19, 1997.*